doi:10.1016/j.jmb.2009.06.061 J. Mol. Biol. (2009) 391, 872–883

JMB

Available online at www.sciencedirect.com

ScienceDirect

ELSEVIER

Deciphering Membrane Insertion of the Diphtheria Toxin T Domain by Specular Neutron Reflectometry and Solid-State NMR Spectroscopy

Alexandre Chenal[1,2,3*†], Lydia Prongidi-Fix[5†], Aurélie Perier[3], Christopher Aisenbrey[5], Grégory Vernier[2], Stephan Lambotte[6], Giovanna Fragneto[4], Burkhard Bechinger[5,6*], Daniel Gillet[3], Vincent Forge[2*] and Michel Ferrand[2*]

[1]*Institut Pasteur, CNRS URA 2185, Unité de Biochimie des Interactions Macromoléculaires, Département de Biologie Structurale et Chimie, 25-28 rue du Dr Roux, 75724 Paris cedex 15, France*

[2]*CEA, DSV, IRTSV, LCBM, CEA Grenoble, 17 av. des Martyrs, F-38054 Grenoble, France*

[3]*CEA, DSV, iBiTecS, SIMOPRO, CEA Saclay, F-91191 Gif sur Yvette, France*

[4]*Institut Laue Langevin, BP 156, rue Jules Horowitz, 38042 Grenoble cedex 9, France*

[5]*Institut de Chimie, Université Louis Pasteur-CNRS UMR7177, 4 rue Blaise Pascal, 67000 Strasbourg, France*

[6]*Max Planck Institute of Biochemistry, Am Klopferspitz 18A, 82152 Martinsried, Germany*

Received 9 February 2009; received in revised form 15 June 2009; accepted 24 June 2009
Available online 1 July 2009

Edited by A. G. Palmer III

Insertion and translocation of soluble proteins into and across biological membranes are involved in many physiological and pathological processes, but remain poorly understood. Here, we describe the pH-dependent membrane insertion of the diphtheria toxin T domain in lipid bilayers by specular neutron reflectometry and solid-state NMR spectroscopy. We gained unprecedented structural resolution using contrast-variation techniques that allow us to propose a sequential model of the membrane-insertion process at angstrom resolution along the perpendicular axis of the membrane. At pH 6, the native tertiary structure of the T domain unfolds, allowing its binding to the membrane. The membrane-bound state is characterized by a localization of the C-terminal hydrophobic helices within the outer third of the *cis* fatty acyl-chain region, and these helices are oriented predominantly parallel to the plane of the membrane. In contrast, the amphiphilic N-terminal helices remain in the buffer, above the polar headgroups due to repulsive electrostatic interactions. At pH 4, repulsive interactions vanish; the N-terminal helices penetrate the headgroup region and are oriented parallel to the plane of the membrane. The C-terminal helices penetrate deeper into the bilayer and occupy about two thirds of the acyl-chain region. These helices do not adopt a transmembrane orientation. Interestingly, the T domain induces disorder in the surrounding phospholipids and creates a continuum of water molecules spanning the membrane. We propose that this local destabilization permeabilizes the lipid bilayer and facilitates the translocation of the catalytic domain across the membrane.

Keywords: diphtheria toxin translocation domain; pH-dependent membrane insertion; specular neutron reflectometry; solid-state NMR spectroscopy

**Corresponding authors.* A. Chenal is to be contacted at Institut Pasteur, Unité de Biochimie des Interactions Macromoléculaires, URA CNRS 2185, Département de Biologie Structurale et Chimie, 25-28, rue du Dr Roux, 75724 Paris cedex 15, France. B. Bechinger, Institut de Chimie, Université Louis Pasteur-CNRS UMR7177, 4 rue Blaise Pascal, 67000 Strasbourg, France. E-mail addresses: alexandre.chenal@pasteur.fr; bechinge@chimie.u-strasbg.fr; vincent.forge@cea.fr; michel.ferrand@cea.fr.

† These authors contributed equally to the experimental work.

Introduction

Diphtheria toxin (DT) is a 58-kDa protein secreted by lysogenic strains of *Corynebacterium diphtheriae*, the causative agent of diphtheria (see Ref. 1 for a review). It consists of three functional domains. During cell intoxication, the receptor-binding (R) domain enables binding of DT to the cell-surface receptor heparin-binding epidermal growth factor. The toxin–receptor complex is internalized into endosomes. Acidification triggers the insertion of the translocation (T) domain into the membrane, which assists the translocation of the catalytic (C) domain across the endosomal membrane. The C domain is released into the cytoplasm with the help of cell proteins,[2,3] where it ADP-ribosylates the elongation factor 2, blocking protein synthesis. DT is used for many medical and biotechnological applications,[4] and a DT–interleukin 2 fusion toxin has been approved for the treatment of lymphomas (see Ref. 5 for review). Deciphering the mechanism of translocation of DT may help to improve the efficiency and safety of fusion toxins, to design strategies aiming at blocking toxin translocation, or to increase the scope of passenger proteins that can be targeted into cells.

The membrane-insertion process of the T domain is one of the most documented among bacterial toxins. However, many conflicting models of the structure of this domain interacting with a membrane have been published (reviewed in Refs. 1 and 6). In solution, the T domain is composed of 10 α-helices, named TH1 to TH9 and TH5′, which are organized in a globular shape.[7] The hydrophobic helices TH8 and TH9 are sandwiched by two layers of amphiphilic helices, TH1 to TH4 and TH5 to TH7. The T domain penetrates membranes *via* a pH-dependent, two-step process.[8–10] As the pH decreases, the protonation of histidine side chains[11] destabilizes the native state of T, which adopts a partially folded, molten-globule state.[9,10,12–14] During the first step of membrane interaction, from pH 7 to pH 6, the solvent-exposed hydrophobic surfaces of the molten-globule state allow interaction and association with the membrane leading to the membrane-bound state.[8–10,14,15] This first step is mainly driven by hydrophobic effects. During the second step, from pH 6 to pH 4, the conformation of the T domain is reorganized, leading to a membrane-inserted state. This step involves a combination of hydrophobic and attractive electrostatic interactions between the T domain and the negatively charged membrane surface.[10,14] The helical content of the T domain is mainly preserved throughout the process.[10] Once in the lipid bilayer, the T domain remains monomeric,[16] permeabilizes the membrane,[10,17] and enables the passage of its N-terminal region from the *cis* to the *trans* side of the membrane.[18] However, despite the wealth of functional data, the details on the pH-dependent membrane structures of DT remain largely unknown.

Neutron reflectivity (NR) is an *in situ* nondestructive tool to extract structural information with angstrom (Å) precision at interfaces.[19–22] The judicious use of samples organized in a single phospholipid bilayer and of the contrast-variation technique has led to the determination of new structural details on the interaction of polypeptides with membranes.[23–30] In particular, NR is a unique technique to study the distribution of mass along the axis perpendicular to the membrane plane. It allows one to identify the successive layers of chemicals composing the lipid bilayer (lipid headgroups and acyl chains), as well as the compounds embedded in the membrane and located in its vicinity (polypeptide and water molecules, for instance; see Fig. 1). In the present study, we took advantage of both the contrast-variation technique and the partial deuterium labeling of the bilayers and of the T domain to simultaneously refine a set of NR profiles, providing unprecedented accuracy and detail on the protein–membrane interactions. Nevertheless, as NR cannot provide information on the secondary structure orientation changes of the membrane-bound proteins, we combined specular NR with solid-state NMR investigations. Solid-state NMR spectroscopy has proved to be a valuable tool for the structural analysis of proteins that are associated with extended lipid bilayers (reviewed, e.g., in Refs. 31–36). In particular, the proton-decoupled ^{15}N solid-state NMR spectra reflect in a direct manner the orientation of polypeptide helices with respect to the plane of the lipid bilayer (see Fig. 1).[37,38] Moreover, solid-state NMR allows probing of the changes of the lipid polar headgroup orientation induced by the interacting protein.[39,40]

Here, a structural model of the pH-dependent T-domain membrane-insertion process is developed from specular NR and solid-state NMR data. We also describe the structural perturbation and hydration changes of the membrane, induced by T-domain insertion. Finally, the implication for the translocation of the C domain during cell intoxication is discussed.

Results

Specular neutron reflectometry

The model membranes, a single phospholipid bilayer composed of 80% dipalmitoyl-phosphatidyl-choline (DPPC) and 20% negatively charged dipalmitoyl-phosphatidyl-acid (DPPA) lipids, were prepared on a silicon substrate, as described in Supplementary Data. At each pH investigated, hydrogen/deuterium ($^1H/^2H$) contrast-variation techniques were used to produce a set of specular NR profiles (Fig. 2). To this aim, membrane bilayers were prepared with acyl chains of three different hydrogen isotopic compositions: membrane made of lipids with (*i*) only hydrogenated acyl chains (^1H only), (*ii*) only deuterated acyl chains (^2H only), and

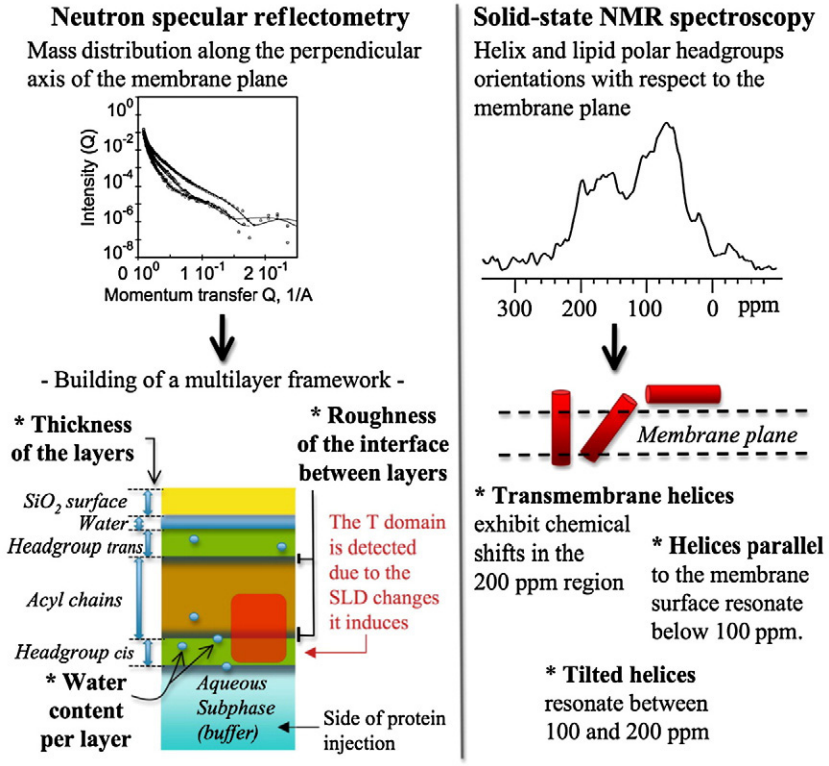

Fig. 1. Schematic representation of the experimental contributions of neutron specular reflectometry and solid-state NMR. Neutron scattering provides information on the mass distribution along the perpendicular axis of the membrane plane. The structural parameters correspond to the layer thickness and hydration, interlayer roughness, and scattering length density (SLD), which is specific of the chemical composition of the layer. Solid-state NMR spectroscopy provides information on the orientations of both the helices (^{15}N spectrum) and lipid polar headgroups (^{31}P spectrum) with respect to the plane of the membrane. The orientation of the helices depends directly on the chemical shift of the ^{15}N resonances, ranging around 200 ppm (transmembrane helices), between 200 and 100 ppm (tilted helices), and below 100 ppm (helices parallel to the membrane surface).

(*iii*) deuterated acyl chains in the *trans* leaflet and hydrogenated acyl chains in the *cis* leaflet ($^2H_{trans}$:$^1H_{cis}$). The membranes, made of the three different isotopic compositions, were each studied at four different contrast-matching conditions of water subphases by varying the D_2O/H_2O ratio (Tables 2 and 3). We first characterized the pure lipid bilayers at pH 7.4, pH 6, and pH 4. The pH of the free-subphase volume (7 mL) of the measuring cell was equilibrated by injections of 20 mL of phosphate-buffered saline adjusted at the targeted pH with acetate buffer (see Supplementary Data for details). All NR experiments were performed at 43 °C (under the control of a temperature bath) to ensure a fluid state of the membrane. All buffer and protein solutions were preheated at 43 °C prior to *in situ* injection in the aqueous subphase of the measurement cell (Fig. 1).

Specular NR intensity curves arose from constructive interferences of the reflected beams from the surface and the interfaces of the successive layers composing the sample (see Supplementary Data Part II.2 for details). The momentum transfer Q being in reciprocal space, the structural parameters and the scattering length density (SLD; defined below) of each layer of the sample were fitted in the framework of a five-layer model to the reflectivity profiles obtained for membranes made of ^1H or ^2H acyl chains and in the framework of a six-layer model for a membrane made of $^2H_{trans}$:$^1H_{cis}$ acyl chains. The distribution of compounds in the multilayer framework is illustrated in Fig. 1 and Fig. S5.

A layer is defined as a homogeneous region (acyl chain or lipid headgroup, for instance) characterized by a set of four parameters (i.e., three structural parameters and its SLD): (*i*) the layer thickness corresponds to the average length of a layer; (*ii*) the layer roughness is the width of the interface between two adjacent layers; (*iii*) the water content is the volume fraction occupied by water (Fig. 1; see Supplementary Data Part II.2). The SLD, which can be considered as a neutron refractive index, is determined by the chemical composition of the layer. It is noteworthy that the SLD is mainly sensitive to hydrogen isotopes (^1H and ^2H; see the atomic coherent neutron-scattering length values in the legend to Table 2). Hence, buffers prepared with different ratios of D_2O/H_2O, as well as the chemical compositions of the lipid acyl chains (^1H or ^2H) and of the polar lipid headgroups regions, in the presence or not of polypeptide, give specific SLD values [see Supplementary Eq. (6) and Tables 2 and 3]. The parameters used to model the reflectivity

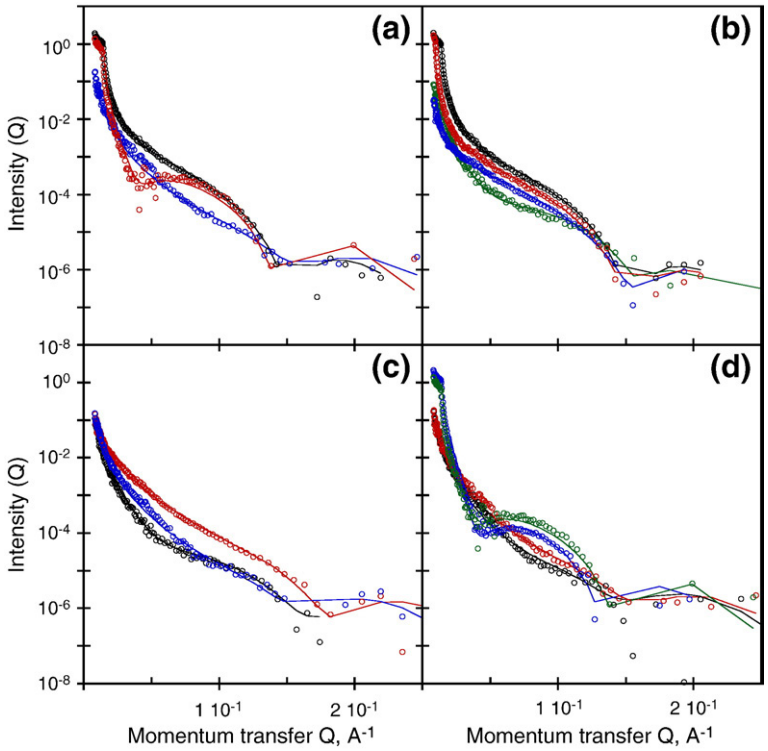

Fig. 2. Specular neutron reflectivity profiles of the T domain in membrane. (a) NR profiles of pure (in the absence of T) membrane bilayers made of DPPC/DPPA 8:2 lipids prepared with a distribution of $^{2}H_{trans}$:$^{1}H_{cis}$ acyl chains (red and blue) and with lipids made of ^{1}H acyl chains only (black) are shown as examples. Phosphate-buffered saline was prepared in D_2O (red and black) and H_2O (blue). (b) NR profiles of membranes made of ^{1}H acyl chains in the presence of T at neutral pH. Contrast-matching conditions were achieved using D_2O/H_2O ratios of 100:0 (black), 69:31 (red), 38:62 (blue), and 0:100 (green). (c) NR profiles of phospholipid bilayers in the presence of T at pH 6 using H_2O as solvent. Membranes were prepared with lipids made of $^{2}H_{trans}$:$^{1}H_{cis}$ (blue), only ^{2}H (red), and only ^{1}H (black) acyl chains. (d) NR profiles of membranes made of $^{2}H_{trans}$:$^{1}H_{cis}$ acyl chains at pH 4. NR profiles in the presence of T (blue and dark) and in its absence (red and green), in H_2O (black and red), and in D_2O (blue and green).

profiles are shown in Table 1 and Table S4. For a given pH, the SLD of a layer is different due to various contrast-matching conditions, but the structural parameters are the same because NR profiles arise from the same biophysical state. $^{1}H/^{2}H$ contrast variations based on D_2O/H_2O ratio (Fig. 2a, b, and d) and acyl-chain composition (Fig. 2c) are illustrated in Fig. 2. Hence, the use of contrast-matching conditions constrains the fits, allowing the assembly of a unique multilayer model of the membrane bilayer derived from a coherent set of NR profiles (Table 1).[24] In the data analysis process and choice of model that best fitted the data, the parts of the NR profiles measured with better statistics ($Q<0.2$ Å^{-1}) were given a higher weight than data with poor statistics (typically at low reflectivities/high Q, i.e., for $Q>0.2$ Å^{-1}).

Structure of the pure lipid bilayer membrane from neutron data

In the absence of protein, the system consisted of the silicon oxide (SiO_2) layer from the silicon substrate, the adsorbed lipid bilayer, and aqueous buffer (Fig. 2a and Table 1). The silicon oxide layer was found to be a single layer of 10±2-Å thickness and a roughness of 4 Å. A water layer separating the lipid bilayer from the polar silicon oxide layer constituted a thin but distinguishable layer of 5± 2-Å thickness. The lipid bilayer was divided into three layers: a *trans* and a *cis* lipid headgroup region of 9±2 Å each, with a hydration comprised between 5% and 8%, separated by a hydrophobic acyl-chain region of 32±2 Å, composed of two leaflets of 16±1 Å (see illustration in Fig. 1). These results are in agreement with data published previously.[41,42] We showed that the structural parameters of the DPPC/DPPA membranes were independent of the pH of the medium (data not shown). The structural parameters of the phospholipid bilayers were then used as references to investigate the conformation of the T domain at each step of the membrane-insertion process.

Conformational changes of the T domain during the membrane-insertion process

For all neutron-scattering experiments described below, we produced and used a T domain labeled uniformly with ^{2}H with the exception of ^{1}H lysine, called the ^{1}HLys ^{2}HT domain. The asymmetrical distribution of lysines along the T-domain sequence allows to distinguish the N-terminal (containing 12/13 lysines) from the C-terminal part (see Table 3). Seven milliliters of a T-domain solution was injected at 7 nM in the free subphase of the measuring cell. This corresponded to 50 pmol injected and to a lipid/protein mol/mol ratio of 660 (see Supplementary Data for details). The NR profiles of ^{1}HLys ^{2}HT domain in the presence of membranes composed of ^{1}H, ^{2}H, and $^{2}H_{trans}$:$^{1}H_{cis}$ acyl chains were recorded at pH 7.4, pH 6, and pH 4, at various water contrast-matching conditions, adjusted by varying the D_2O/H_2O ratio (Fig. 2b

Table 1. Averaged structural parameters [thickness (Å), roughness (Å), and water content (%)] determined from the neutron reflectivity profiles of membranes alone and in the presence of the T domain at pH 7.4, pH 6, and pH 4 fitted to the multilayer framework model

Layer	Composition	Thickness	Roughness	Water
Membrane without protein				
1	SiO_2	10	4	0
2	Water	5	6	100
3	*trans* PH	9	6	5
4	HC	32	6	2
5	*cis* PH	9	6	8
Membrane in the presence of T at pH 7.4				
1	SiO_2	10	3	0
2	Water	5	7	100
3	*trans* PH	9	7	5
4	HC	32	4	7
5	*cis* PH	9	7	17
Membrane in the presence of T at pH 6				
1	SiO_2	11	4	0
2	Water	6	6	100
3	*trans* PH	8	7	5
4	HC	24	8	11
5	HC+ T	9	6	12
6	*cis* PH	9	5	40
Membrane in the presence of T at pH 4				
1	SiO_2	10	5	0
2	Water	6	5	100
3	*trans* PH	9	5	16
4	HC	15	6	12
5	HC+ T	21	8	23
6	*cis* PH+ T	8	6	47

PH, polar headgroups, HC, hydrophobic core; T, T domain; HC+ T, layer containing both acyl chains and part of the T domain. SDs of thickness, roughness, and hydration are ±2 Å, ±2 Å, and ±5%, respectively.

and d). The NR curves were analyzed as stacked multilayers and progressively refined from pH 7.4 to pH 4 by introducing realistic modifications in the structural parameters determined for the pure lipid bilayers described above. Hence, the interactions of the T domain with the lipid bilayer were detected by the perturbations it induced on the SLD and the structural parameters of each layer of the membrane (Fig. 1). NR profiles of the T domain at neutral pH are shown in Fig. 2b. The results presented in Table 1 indicate that the T domain induced only minor modifications of the structural parameters. Indeed, only the hydration of the *cis* polar headgroup exhibited a detectable increase of 10%. Hence, at neutral pH, the T domain is likely not to be tightly bound to the membrane, in agreement with previous results,[10,13,14] although it resided in the vicinity of the lipid polar headgroups, as revealed by the hydration increase of this region.

The pH was then lowered to 6 by addition of acetate buffer in the free subphase of the measuring cells. The NR curves were recorded and the structural parameters were fitted in the same multilayer framework model as in the absence of T (Table 1 and Table S4). The effects of T on the three membranes for the same buffer are shown in Fig. 2c. The first three layers—silicon oxide, water layer, and *trans* lipid polar headgroups—showed similar structural parameters as in the absence of the protein, indicating that they were insensitive to the presence of the T domain at pH 6 (Table 1). For each reflectivity curve, an additional layer was introduced in the multilayer framework to fit to the data: the acyl-chain region had to be separated into two layers to match the SLD changes (see Fig. S5). The fourth layer, 24±2 Å thick, corresponded to pure acyl chains alone, as shown by the preservation of the molecular SLD of pure acyl chains for the three ^1H, ^2H, and $^2H_{trans}$:$^1H_{cis}$ acyl-chain isotopic compositions investigated (Table S4). The fifth layer corresponded to a combination of acyl chains and protein of 9±2-Å thickness (Table 1). The contribution of the T domain to this SLD layer fitted, for the 12 contrast conditions studied, to the TH5–TH9 molecular SLD, which contained only one ^1H lysine (see Table 3). The thickness of this layer (9 Å) is incompatible with a transmembrane orientation of the T-domain helices. It is noteworthy that the presence of the T domain induced a weak increase of hydration of the pure acyl-chain layer, although the protein was clearly absent from this region.

Finally, the last layer, corresponding to the *cis* lipid headgroup region, exhibited a thickness similar to that in the absence of the T domain. The SLD was only weakly affected by the presence of the T domain (Table S4). Interestingly, this indicated that the T domain (particularly its N-terminal part with a high molecular SLD due to the 12 ^1HLys residues) did not reside in this region of the membrane. Hence, the N-terminal part of the T domain should be localized beyond the *cis* lipid headgroup region, i.e., in the buffer, where the helices are too hydrated and too dynamic to be detected by neutron reflectometry. Moreover, it was noteworthy that the presence of the N-terminal part of the T domain close to the *cis* lipid headgroup area induced a strong increase of hydration of this layer to 40%, compared to 8% for pure membrane and 17% in the presence of the T at neutral pH. The hydration increase may also arise from the segment(s) of T that penetrated this region, linking the N- and C-terminal parts of the protein.

Taken together, the results showed that the *trans* polar headgroups and two thirds of the hydrophobic core were not affected by the presence of the T domain at pH 6. Its C-terminal part penetrated the membrane among the first methylene groups of the *cis* acyl-chain region. The *cis* lipid headgroup region was mostly free of protein and highly solvated. This is probably due to the proximity of the N-terminal part of the T domain that remained solvent exposed outside the membrane.

The pH of the sample cells was then decreased to 4 to investigate the membrane-inserted state of the T domain. The NR profiles were measured and the structural parameters fitted using the multilayer framework model described above. The comparison of NR profiles of the membrane alone or in the presence of the protein at pH 4 showed profound modifications of the system (Fig. 2d). Similarly, the NR profiles clearly indicated that the effect of T on

Table 2. Scattering length densities of lipids used in this study (in H_2O buffer)

Lipid parts	Chemical structure	SLD[a] ($\times 10^{-6}$ Å^{-2})	Experimental SLD
Polar headgroup of DPPC	$C_{10}H_{18}NO_8P$	1.25	—
Polar headgroup of DPPA	$C_5H_6O_8P$	1.3	—
Polar headgroups mixing (CH chains)	DPPC/ DPPA 8:2	1.26	1.29
Polar headgroups mixing (CD chains)	DPPC/ DPPA 8:2	1.26	2.3[b]
Deuterated hydrophobic tails	$C_{30}D_{62}$	6.1	6.4
Hydrogenated hydrophobic tails	$C_{30}H_{62}$	−0.32	−0.29

[a] The SLD values were calculated by dividing the molecular coherent neutron scattering length B_{mol} by the molecular volume V_M. The B_{mol} was calculated using the atomic coherent neutron scattering length values of ^{1}H (-3.74×10^{-5} Å), ^{2}H (6.67×10^{-5} Å), C (6.65×10^{-5} Å), N (9.36×10^{-5} Å), O (5.80×10^{-5} Å), S (2.85×10^{-5} Å), and P (5.13×10^{-5} Å). V_M of polar headgroups and hydrophobic tails were 480 and 1000 Å^3, respectively. The experimental SLD values were determined with the neutron reflectivity curves of membranes in the absence of protein (see Materials and Methods).

[b] The SLD layer of 2.3×10^{-6} Å^{-2} is due to the occurrence of a fraction of 0.2 deuterated carbons (CD) from acyl chain in the polar headgroup [see Supplementary Eqs. (5) and (6) for details].

the membrane increased as the pH decreased, as shown in Fig. S6. At pH 4, only the silicon substrate and its hydration layer were not affected (Table 1). The *trans* polar headgroup region (layer 3) became highly solvated but there was no evidence of the presence of the T domain crossing the lipid bilayer. Indeed, the SLD of this layer was characteristic of a pure lipid headgroup composition.

The structural parameters deduced from the ^{2}H-only and the $^2H_{trans}$:$^1H_{cis}$ acyl-chain isotopic compositions of the membranes indicated that the acyl-chain region was heterogeneous. Layer 4 was composed of pure acyl chains. Its thickness (15 Å) was thinner than at pH 6 (24 Å). Layer 5 contained a combination of acyl chains and T domain (reflected by the SLD of the layer). Its thickness (21 Å) was larger than at pH 6 (9 Å). The data showed the progressive pH-dependent membrane insertion of the C-terminal part of the T domain, which induced a swelling of the acyl-chain region. Indeed, the hydrophobic core thickness was 32 Å in the absence of T, 33 Å in its presence at pH 6, and 36 Å in its presence at pH 4.

Layer 6, corresponding to the polar lipid headgroups, was the most hydrated region of the membrane. It is noteworthy that the layer's SLD allowed us to assign the N-terminal part of the T domain to this region. This observation is supported by the following facts. The expected SLD for pure lipid headgroups in D_2O was 2.3×10^{-6} Å^{-2} and the experimental SLD was 3×10^{-6} Å^{-2} (see Tables 2 and 3 and Table S4). The only way to increase the SLD was (*i*) the densification of the layer by compaction of the lipid headgroups induced by the insertion of molecules and/or (*ii*) the mixing of lipid headgroups with materials of higher SLD. The N-terminal part of the ^{1}HLys T domain had a SLD higher than 3×10^{-6} Å^{-2} whatever the contrast-matching conditions, while the SLD of the C-terminal part was below 3×10^{-6} Å^{-2} (Table 3). Hence, only the insertion of the N-terminal part of the T domain in the polar lipid headgroup region may explain the observed variation of the SLD. Finally, a common feature of all layers at pH 4 was the dramatic increase of the water content throughout the lipid bilayer induced by the insertion of the T domain. This increase of water content was clearly pH dependent.

Overall, the results showed that the T domain progressively penetrated the membrane as the pH decreased. The membrane-bound state at pH 6 was characterized by a 9-Å-deep insertion of the C-terminal part of the protein into the *cis* acyl-chain region, while its N-terminal part remained solvent exposed beyond the polar lipid headgroups. The C-terminal part of the protein penetrated deeper (21 Å) the hydrocarbon core at pH 4. Meanwhile, the N-terminal part of T partitioned from the solvent to the polar headgroup region. The insertion of the T domain induced a swelling of more than 10% of the hydrocarbon core and an increase of membrane hydration spanning the bilayer from side to side.

Solid-state NMR spectroscopy

The T domain was labeled uniformly with ^{15}N and reconstituted into uniaxially oriented phospholipid membranes, composed of palmitoyl-oleoyl phosphatidyl-choline (POPC)/palmitoyl-oleoyl phosphatidyl-glycerol (POPG) at a 8:2 molar ratio at either pH 6 or pH 4 (see Supplementary Data Part 2). We showed that the T domain behaved similarly in the presence of phosphatidyl-glycerol or phosphatidic acid as anionic lipids (see Supplementary text and Fig. S7). At each pH investigated, samples were equilibrated at 100% relative humidity (r.h.) to optimize the comparison with the NR data, which were obtained with a semi-infinite free-subphase volume.

In a first step, the oriented samples were investigated by proton-decoupled ^{31}P NMR spectroscopy as this approach provides an estimate of the alignment order of the phospholipid headgroups.[43] Whereas liquid crystalline phosphatidylcholine bilayers with their long axis oriented parallel to the

Table 3. Calculated scattering length densities of water, the T domain, and the N-terminal (TH1–TH4) and the C-terminal (TH5–TH9) parts of the T domain

	Scattering length densities[a] ($\times 10^{-6}$ Å^{-2})			
Water composition	Whole T domain	TH1–TH4	TH5–TH9	Subphase water
D_2O	3.14	3.80	2.72	6.36
H_2O	2.39	3.08	1.94	−0.56
38% D_2O	2.72	3.35	2.24	2.07
69% D_2O	2.91	3.57	2.49	4.21

[a] The SLD values were calculated by dividing the molecular coherent neutron scattering length B_{mol} by the molecular volume V_M. The B_{mol} was calculated using the atomic coherent neutron scattering lengths given in Table 2.

magnetic field direction exhibit resonances at about 30 ppm, signals below 30 ppm arise from phospholipid headgroups with orientations deviating from this alignment. At the other extreme, a signal at −15 ppm corresponds to phosphatidylcholines with their long axis perpendicular to the magnetic field direction.

The ^{31}P solid-state NMR spectra of the pure membranes showed a peak in the 30-ppm region, which arose from the overlapping resonances of POPC and POPG aligned with their long axes perpendicular to the glass plates (Fig. 3a). This peak position is indicative of well-oriented phospholipid membranes in their liquid crystalline state. In the presence of the protein and at pH 4, a fraction of the phospholipid resonance, probably the signal arising from POPG, is shifted to 19 ppm (Fig. 3b). This observation suggested that electrostatic effects between POPG lipids and the T domain affected the lipid polar headgroup conformation and/or packing. Furthermore, depending on the detailed experimental conditions, the presence of the T domain caused additional ^{31}P NMR intensities between 30 and −15 ppm, indicative of a more heterogeneous alignment of the headgroup region relative to the glass-plate normal (Fig. S8).

In a second step, the samples were investigated by proton-decoupled ^{15}N solid-state NMR spectroscopy, which monitors the topology and dynamics of the ^{15}N-labeled sites of the protein (Fig. 3c–f). As the T domain was labeled uniformly with ^{15}N, this signal arose from 199 amide bonds as well as contributions from the lysine, arginine, asparagine, histidine, and tryptophan side chains.[44] Whereas side chains that undergo fast reorientational dynamics are, to a great extent, filtered out by the cross-polarization sequence, backbone amides that are immobilized by interactions with the membrane exhibit orientation-dependent ^{15}N chemical-shift values.[38] Whereas α-helical domains with alignments parallel to the membrane surface resonate below 100 ppm, transmembrane helices exhibit chemical shifts in the 200-ppm region (see Fig. 1). The technique has therefore been used to monitor the helix alignment of peptides and proteins.[37,45]

The proton-decoupled cross-polarization ^{15}N solid-state NMR spectrum of the T domain bound to POPC/POPG 8:2 (wt/wt) membranes at pH 6 and at 100% or 93% r.h. showed that the main signal intensities were in the 120–60 ppm region (Fig. 3c and e), indicative of a distribution of alignments of the NH vectors. The proton-decoupled ^{15}N solid-state NMR spectra were deconvoluted into Gaussian functions to estimate the contribution from in-plane, tilted/transmembrane orientations. The envelope of NH resonances above 120 ppm was low, covering only 30% of the transmembrane signal intensity at 93% r.h. (Fig. 3e), and about 20–25% of the total signal intensity was centered around 135 ppm at full hydration (Fig. 3c). The strong intensities below 120 ppm indicated that the membrane-bound helices of the T domain adopted an orientation predominantly parallel to the lipid bilayer plane (Fig. 3c and e). A spectrum of the sample at full hydration was then recorded at pH 6 using a Hahn-echo pulse sequence to detect in a more quantitative manner the resonances from nitrogen atoms undergoing a high degree of motion. Under these experimental conditions (100% r.h. and pH 6), the peak located at 125 ppm was considerably more pronounced and corresponded to the resonance of amide residues and some of the side chains evolving in an isotropic environment (i.e., in the aqueous phase between the membrane layers of the sample; Fig. S9 and Ref. 46). Consequently, such mobile residues were not constrained in the anisotropic membrane milieu, suggesting that large parts of the protein reoriented in the aqueous environment as they were only loosely bound to the lipid bilayers. In a similar manner, the Hahn-echo pulse sequence strongly enhanced signal intensities at 175 and 37 ppm, where the isotropic histidine and lysine side-chain intensities are expected (Fig. S9 and Ref. 44).

Proton-decoupled ^{15}N solid-state NMR spectra of the membrane-inserted T domain at pH 4 and at 100% r.h. (Fig. 3d) exhibited a line shape with about 20% of the total signal intensity occurring in the spectral region around 165 ppm, thereby indicating a more stable insertion of tilted protein helices into the membrane when compared to that at pH 6 (Fig. 3c). Nevertheless, the strong intensity of the chemical shifts centered around 90 ppm at pH 4 indicated that most helices (about 80% of the total intensity) still adopted an orientation in the plane of the lipid bilayer (Fig. 3d). The spectra of the samples at pH 6 and pH 4 equilibrated at 93% r.h. are shown in Fig. 3e and f. Under these conditions, the predominantly in-plane alignment of helices was retained. At pH 4 and 93% r.h., resonances indicative of transmembrane and tilted helices increased to about 40% of the total signal intensities (Fig. 3f) and are therefore considerably augmented when compared to that at pH 6 (Fig. 3e) or at full hydration (Fig. 3c and d).

Together, the solid-state NMR data showed that parts of the protein were loosely bound to the membrane at pH 6 at 100% r.h. (Fig. S9) and that the membrane-interacting helices were organized predominantly parallel to the bilayer surface. At full hydration, a strong peak around 125 ppm indicated important isotropic motions of a fraction of the T-domain backbone. Moreover, the alignment of the lipid polar headgroups was affected in the membrane-bound state. At acidic pH, the helices remained mostly in the plane of the lipid bilayer, although an augmentation in the ratio of transmembrane or oblique helix alignments is observed (chemical shifts between 100 and 200 ppm). Hence, it is noteworthy that a large fraction of helices was organized in the plane of the bilayer whatever the pH investigated.

Discussion

We have investigated the pH-dependent membrane-insertion process of the isolated T domain of the DT in order to gain new insights in the

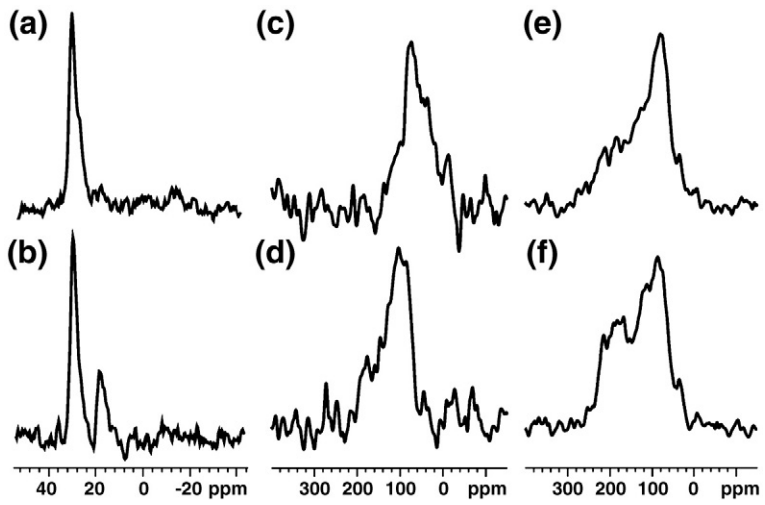

Fig. 3. Proton-decoupled ^{31}P solid-state NMR spectra of (a) POPC/POPG (8:2 mol/mol) membranes at pH 6 oriented with their membrane normal parallel to the magnetic field direction and (b) of a sample prepared in a similar manner containing the DT T domain at a protein-to-lipid ratio of 1:40 (wt/wt) at pH 4. Panels c–f show proton-decoupled cross-polarization ^{15}N spectra of the T domain at pH 6 (c and e) and pH 4 (d and f) reconstituted into oriented POPC/POPG (8:2 mol/mol) membrane at a protein-to-lipid ratio of 1:40 (wt/wt) and equilibrated at 100% r.h. (a–d) or 93% r.h. (e and f) before the NMR measurements.

mechanism leading to the translocation of the C domain of the toxin across the endosomal membrane. In this study, we resorted to two different methods: (*i*) specular neutron reflectometry, which allows one to obtain information on the structural parameters (thickness, roughness, and hydration) of the membrane and on the location of polypeptide segments inserted in the lipid headgroup and acyl-chain regions of the membrane, and (*ii*) solid-state NMR spectroscopy, which provides information on the orientation of helices of the protein with respect to the membrane plane (Fig. 1). Our results allow us to propose a structural model of the conformational changes of the T domain from its soluble state to its membrane-bound state and finally to its membrane-inserted state. Furthermore, we describe the structural, dynamic, and hydration changes of the lipid bilayer induced by the interaction with the T domain. From these data, we propose a model that summarizes our findings (Fig. 4).

At neutral pH, the native state of T in solution is characterized by stable secondary and tertiary structures.[10,13] In the presence of a membrane, the T domain remains in the aqueous buffer but is transiently close to the membrane surface, as revealed by the weak increase of hydration of the *cis* lipid polar headgroups detected by neutron scattering. At pH 6, the T domain is accumulated in the membrane-bound state. Specular NR experiments show that the protein–membrane interaction involves the anchoring of the C-terminal part of T, which occupies the first 9 Å of the *cis* acyl-chain region (i.e., below the *cis* polar headgroups). The results suggest that the C-terminal helices are those detected parallel to the bilayer surface by solid-state NMR spectroscopy. The N-terminal part of T remains solvent exposed beyond the *cis* lipid polar headgroups: it is too dynamic to be observed by neutron scattering and may correspond to the loosely membrane-bound fraction, which exhibits dynamic movements in aqueous buffer revealed by the isotropic intensities observed in Hahn-echo solid-state NMR spectra. Accordingly, previous experiments suggested that the N-terminal part of the T domain is exposed to the aqueous buffer in the membrane-bound state.[14] Moreover, Erwin London's group showed that the N-terminal helices form an autonomous region that does not deeply penetrate the membrane,[47] in contrast to the C-terminal part of the T domain that is located in the hydrocarbon core of the membrane.[48] Our observation that the C-terminal helices reside in-plane at the depth of the first methylene groups of the *cis* monolayer, while the N-terminal helices move freely in solution, clearly indicates that the T domain undergoes a large unfolding upon membrane binding. We propose that two opposing effects drive this profound tertiary structure disruption. First, hydrophobic forces between the C-terminal part of T and the acyl chains drive protein–membrane partitioning. Second, the repulsive electrostatic interactions between the anionic polar headgroups and the negatively charged N-terminal part of T preclude membrane insertion of this region. Moreover, these repulsive electrostatic interactions reorganize the lipid polar headgroups and increase their hydration, as measured by ^{31}P NMR and neutron reflectivity, respectively.

At pH 4, dramatic changes occur. Neutron reflectivity experiments provide direct evidence that the C-terminal part of T penetrates deeply the hydrocarbon core and inserts into the upper two thirds of the hydrophobic region, while its N-terminal helices penetrate the polar headgroup region. Interestingly, the helices remain mostly parallel to the membrane surface, an orientation similar to that found at pH 6. Indeed, the NMR data clearly indicate that at 100% r.h., only a small fraction of the ^{15}N NMR signal intensities corresponds to helices that adopt an oblique orientation (Fig. 3d). Furthermore, ^{15}N NMR signal intensities that agree with a transmembrane conformation are observed only at 93% r.h. (Fig. 3f). This observation highlights the propensity of the T domain to switch between conformational states in the membrane in reaction to subtle environmental changes, such as relative humidity, lipid composition of the membrane, or ionic strength.[8,10,14,49] This is in agreement

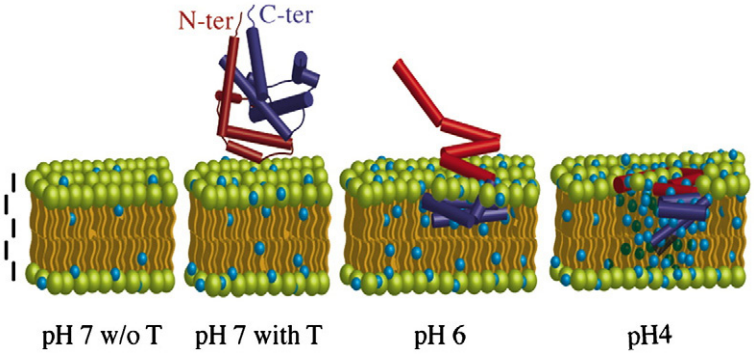

Fig. 4. Scheme of the pH-dependent membrane-insertion process of the DT T domain. From left to right: membrane at pH 7 in the absence of T, membrane at the same pH in the presence of T, the membrane-bound state of T at pH 6, and the membrane-inserted state of T at pH 4. Membrane layers, the T domain, and water molecules are scaled. The water molecules correspond to the water content determined for each layer from neutron experiments. Red and blue cylinders represent the helical backbone of TH1–TH4 and TH5–TH9, respectively. Acyl chains and polar headgroups are yellow and green, respectively. The vertical scale bar represents 1 nm.

with results showing that shallowly and deeply inserted states of the T domain are regulated by the physico-chemical properties of the lipid bilayer.[6,8]

We propose the following folding pathway to describe the transition from the membrane-bound state to the membrane-inserted state. The repulsive electrostatic interactions, keeping the N-terminal part of T away from the membrane surface at pH 6, may prevent deep insertion of the C-terminal helices, which reside in-plane within the first 9 Å of the *cis* acyl-chain region. The protonation of acidic residues, induced by the drop of pH from 6 to 4, abolishes repulsive electrostatic interactions between the negatively charged membrane and the N-terminal helices of T. These helices then start to partition from the aqueous buffer to the polar headgroup region through hydrophobic effects and attractive electrostatic interactions between basic amino-acid side chains and the anionic polar headgroups. This allows the C-terminal part of T to reach a deeper position in the hydrophobic milieu, where it finally reaches 21 Å below the *cis* polar headgroups. The membrane-inserted state we describe here might be the conformation accumulated before the N-terminal helices cross the membrane[18] and help the translocation of the C domain.[50,51] It is noteworthy that we did not show the accumulation of the N-terminal helices in the trans side of the membrane. This could be due to several factors, such as steric hindrance in the trans side, the absence of a pH gradient,[52,53] or the lack of proteins contributing to the translocation process.[2,54,55]

The membrane-inserted state of the T domain induces a swelling of 4 Å of the acyl-chain region. This swelling probably reflects the increase of the membrane volume induced by the insertion of T and the additional presence of water molecules. Indeed, an unexpected observation of this study is the progressive increase of membrane hydration as the pH decreases in the presence of the T domain. These results strongly suggest that membrane impermeability is locally disrupted by the presence of T at acidic pH. In addition, this probably reflects the pH-dependent ability of T to permeabilize the membrane.[10,17]

These data provide new insights into the events preceding the translocation of the C domain of DT during cell intoxication. We showed that the membrane-insertion process of T induces rearrangements in polar headgroups and hydration increase throughout the lipid bilayer, leading to local membrane destabilization. Nevertheless, our results indicate that T does not materially form a proteinaceous pore from the *cis* to the *trans* side of the lipid bilayer. We propose that the membrane-destabilizing effect of T produces a continuum of water molecules across the membrane, comparable to observations made with antimicrobial[40,56] or cell-penetrating peptides.[57,58] In the physiological context, the membrane-inserted state of the T domain might create a water-filled pathway across the membrane of the endosome. Once the N-terminal helices of T reach the cytosol, due to the pH gradient across the endosomal membrane,[10,18] cytosolic proteins (such as HSP90 and COP proteins) bind helix TH1.[2,3,59,60] These TH1-bound proteins might prevent any backward movement of the N-terminal part of T into the endosome. Such cytosolic complex might contribute to complete the translocation by a molecular ratchet process by extruding C from the membrane. We propose that the membrane-inserted T domain favors the passage of the C domain from the endosome to the cytoplasm because the energy required for a partially folded domain to cross a locally destabilized membrane should be lower than that necessary to cross a stable lipid bilayer barrier. In other words, the T domain might facilitate the translocation of C by coupling membrane insertion to membrane destabilization.

Materials and Methods

Protein production and purification

The recombinant isolated T domain of the DT used in this study has been described elsewhere.[10] Lipids were purchased from Avanti Polar Lipids and used as received.

Specular neutron reflectometry

The measurements were performed on the D17 reflectometer at the Institut Laue Langevin (Grenoble, France). The reflectometer was set up in time-of-flight mode using a spread of wavelengths between 2 and 20 Å with two

incoming angles of 0.7° and 2.4°. The NR profiles were model fitted to obtain the structural parameters.[29]

NMR spectroscopy

Samples were investigated using flat-coil solid-state NMR probe heads introduced into the magnetic field of a Bruker Advance wide-bore NMR spectrometer operating at 9.4 T. ^{31}P and ^{15}N solid-state NMR spectra were obtained following the protocols described elsewhere.[37,43]

All experimental procedures are described in detail in Supplementary Data.

Acknowledgements

The authors thank Institut Laue Langevin for beam-time; Sylvain Pichard and Pascal Belin for the auxotrophic BL21 strain; Nicolas Gilles and Marie Courçon for fermentor production; Marie-Thérèse Dauvergne and Michael Haertlein from the Deuteration Laboratory for the production of the deuterium-labeled protein; Roya Barumandhez for help with sample preparation and neutron experiments; and Bernard Sartor for designing and building the neutron cells. A.C. was supported by the Ligue Nationale contre le Cancer and by Action Concertées Incitative-microbiology program of Fonds National de la Science Grant MIC 0325. The financial support by Vaincre la mucoviscidose is gratefully acknowledged (grant to L.P.F.). We thank Agnès Ullmann and Patrick England for critical reading of the manuscript. The Bechinger group is grateful to be hosted by the Institute of Supramolecular Chemistry at the University of Strasbourg.

Supplementary Data

Supplementary data associated with this article can be found, in the online version, at doi:10.1016/j.jmb.2009.06.061

References

1. Chenal, A., Nizard, P. & Gillet, D. (2002). Structure and function of diphtheria toxin: from pathology to engineering. *J. Toxicol., Toxin Rev.* **21**, 321–359.
2. Ratts, R., Zeng, H., Berg, E. A., Blue, C., McComb, M. E., Costello, C. E. *et al.* (2003). The cytosolic entry of diphtheria toxin catalytic domain requires a host cell cytosolic translocation factor complex. *J. Cell Biol.* **160**, 1139–1150.
3. Ratts, R., Trujillo, C., Bharti, A., vanderSpek, J., Harrison, R. & Murphy, J. R. (2005). A conserved motif in transmembrane helix 1 of diphtheria toxin mediates catalytic domain delivery to the cytosol. *Proc. Natl Acad. Sci. USA*, **102**, 15635–15640.
4. Nizard, P., Gross, D. A., Babon, A., Chenal, A., Beaumelle, B., Kosmatopoulos, K. & Gillet, D. (2003). Anchoring cytokines to tumor cells for the preparation of anticancer vaccines without gene transfection in mice. *J. Immunother.* **26**, 63–71.
5. Perier, A., Chenal, A., Babon, A., Ménez, A. & Gillet, D. (2005). Engineering of bacterial toxins for research and medicine. In *Comprehensive sourcebook of bacterial protein toxins* (Alouf, J. E. & Popoff, M. R., eds), 3rd edit. Academic Press, London.
6. Zhao, G. & London, E. (2005). Behavior of diphtheria toxin T domain containing substitutions that block normal membrane insertion at Pro345 and Leu307: control of deep membrane insertion and coupling between deep insertion of hydrophobic subdomains. *Biochemistry*, **44**, 4488–4498.
7. Bennett, M. J., Choe, S. & Eisenberg, D. (1994). Refined structure of dimeric diphtheria toxin at 2.0 A resolution. *Protein Sci.* **3**, 1444–1463.
8. Wang, Y., Malenbaum, S. E., Kachel, K., Zhan, H., Collier, R. J. & London, E. (1997). Identification of shallow and deep membrane-penetrating forms of diphtheria toxin T domain that are regulated by protein concentration and bilayer width. *J. Biol. Chem.* **272**, 25091–25098.
9. Malenbaum, S. E., Collier, R. J. & London, E. (1998). Membrane topography of the T domain of diphtheria toxin probed with single tryptophan mutants. *Biochemistry*, **37**, 17915–17922.
10. Chenal, A., Savarin, P., Nizard, P., Guillain, F., Gillet, D. & Forge, V. (2002). Membrane protein insertion regulated by bringing electrostatic and hydrophobic interactions into play. A case study with the translocation domain of diphtheria toxin. *J. Biol. Chem.* **277**, 43425–43432.
11. Perier, A., Chassaing, A., Raffestin, S., Pichard, S., Masella, M., Menez, A. *et al.* (2007). Concerted protonation of key histidines triggers membrane interaction of the diphtheria toxin T domain. *J. Biol. Chem.* **282**, 24239–24245.
12. D'Silva, P. R. & Lala, A. K. (1998). Unfolding of diphtheria toxin. Identification of hydrophobic sites exposed on lowering of pH by photolabeling. *J. Biol. Chem.* **273**, 16216–16222.
13. Chenal, A., Nizard, P., Forge, V., Pugniere, M., Roy, M. O., Mani, J. C. *et al.* (2002). Does fusion of domains from unrelated proteins affect their folding pathways and the structural changes involved in their function? A case study with the diphtheria toxin T domain. *Protein Eng.* **15**, 383–391.
14. Montagner, C., Perier, A., Pichard, S., Vernier, G., Menez, A., Gillet, D. *et al.* (2007). Behavior of the N-terminal helices of the diphtheria toxin T domain during the successive steps of membrane interaction. *Biochemistry*, **46**, 1878–1887.
15. D'Silva, P. R. & Lala, A. K. (2000). Organization of diphtheria toxin in membranes: a hydrophobic photolabeling study. *J. Biol. Chem.* **275**, 27500.
16. Gordon, M. & Finkelstein, A. (2001). The number of subunits comprising the channel formed by the T domain of diphtheria toxin. *J. Gen. Physiol.* **118**, 471–480.
17. Sharpe, J. C. & London, E. (1999). Diphtheria toxin forms pores of different sizes depending on its concentration in membranes: probable relationship to oligomerization. *J. Membr. Biol.* **171**, 209–221.
18. Senzel, L., Gordon, M., Blaustein, R. O., Oh, K. J., Collier, R. J. & Finkelstein, A. (2000). Topography of diphtheria toxin's T domain in the open channel state. *J. Gen. Physiol.* **115**, 421–434.
19. Penfold, J. & Thomas, R. K. (1990). The application of the specular reflection of neutrons to the study of

surfaces and interfaces. *J. Phys. Condens. Matter*, **2**, 1369–1412.
20. Russell, T. P. (1990). X-ray and neutron reflectivity for the investigation of polymers. *Mater. Sci. Rep.* **5**, 171–271.
21. Daillant, J. & Gibaud, A. (1999). *X-Ray and Neutron Reflectivity: Principles and Applications*. Springer, Berlin.
22. Majewski, J., Kuhl, T. L., Wong, J. Y. & Smith, G. S. (2000). X-ray and neutron surface scattering for studying lipid/polymer assemblies at the air–liquid and solid–liquid interfaces. *J. Biotechnol.* **74**, 207–231.
23. Bradshaw, J. P., Davies, S. M. & Hauss, T. (1998). Interaction of substance P with phospholipid bilayers: a neutron diffraction study. *Biophys. J.* **75**, 889–895.
24. Fragneto, G., Graner, F., Charitat, T., Dubos, P. & Bellet-Amalric, E. (2000). Interaction of the third helix of antennapedia homeodomain with a deposited phospholipid bilayer: a neutron reflectivity structural study. *Langmuir*, **16**, 4581–4588.
25. Majkrzak, C. F., Berk, N. F., Krueger, S., Dura, J. A., Tarek, M., Tobias, D. *et al.* (2000). First-principles determination of hybrid bilayer membrane structure by phase-sensitive neutron reflectometry. *Biophys. J.* **79**, 3330–3340.
26. Krueger, S., Meuse, C. W., Majkrzak, C. F., Dura, J. A., Berk, N. F., Tarek, M. & Plant, A. L. (2001). Investigation of hybrid bilayer membranes with neutron reflectometry: probing the interactions of melittin. *Langmuir*, **17**, 511–521.
27. Salditt, T., Münster, C., Mennicke, U., Ollinger, C. & Fragneto, G. (2003). Thermal fluctuations of oriented lipid membranes by nonspecular neutron reflectometry. *Langmuir*, **19**, 7703–7711.
28. Jackler, G., Czeslik, C., Steitz, R. & Royer, C. A. (2005). Spatial distribution of protein molecules adsorbed at a polyelectrolyte multilayer. *Phys. Rev. E: Stat. Nonlin. Soft Matter Phys.* **71**, 041912.
29. Vacklin, H. P., Tiberg, F., Fragneto, G. & Thomas, R. K. (2005). Phospholipase A2 hydrolysis of supported phospholipid bilayers: a neutron reflectivity and ellipsometry study. *Biochemistry*, **44**, 2811–2821.
30. Wacklin, H. P., Tiberg, F., Fragneto, G. & Thomas, R. K. (2007). Distribution of reaction products in phospholipase A2 hydrolysis. *Biochim. Biophys. Acta*, **1768**, 1036–1049.
31. Cross, T. A. (1997). Solid-state nuclear magnetic resonance characterization of gramicidin channel structure. *Methods Enzymol.* **289**, 672–696.
32. Griffin, R. G. (1998). Dipolar recoupling in MAS spectra of biological solids. *Nat. Struct. Biol.* **5 Suppl**, 508–512.
33. Davis, J. H. & Auger, M. (1999). Static and magic angle spinning NMR of membrane peptides and proteins. *Prog. Nucl. Magn. Reson. Spectrosc.* **35**, 1–84.
34. Watts, A., Burnett, I. J., Glaubitz, C., Grobner, G., Middleton, D. A., Spooner, P. J. *et al.* (1999). Membrane protein structure determination by solid state NMR. *Nat. Prod. Rep.* **16**, 419–423.
35. Bechinger, B., Aisenbrey, C. & Bertani, P. (2004). The alignment, structure and dynamics of membrane-associated polypeptides by solid-state NMR spectroscopy. *Biochim. Biophys. Acta*, **1666**, 190–204.
36. Hong, M. (2006). Solid-state NMR studies of the structure, dynamics, and assembly of β-sheet membrane peptides and α-helical membrane proteins with antibiotic activities. *Acc. Chem. Res.* **39**, 176–183.
37. Aisenbrey, C., Sudheendra, U. S., Ridley, H., Bertani, P., Marquette, A., Nedelkina, S. *et al.* (2007). Helix orientations in membrane-associated Bcl-X_L determined by ^{15}N-solid-state NMR spectroscopy. *Eur. Biophys. J.* **37**, 71–80.
38. Bechinger, B. & Sizun, C. (2003). Alignment and structural analysis of membrane polypeptides by ^{15}N and ^{31}P solid-state NMR spectroscopy. *Concepts Magn. Reson.* **18A**, 130–145.
39. Seelig, J. (1978). ^{31}P nuclear magnetic resonance and the head group structure of phospholipids in membranes. *Biochim. Biophys. Acta*, **515**, 105–140.
40. Bechinger, B. (1999). The structure, dynamics and orientation of antimicrobial peptides in membranes by multidimensional solid-state NMR spectroscopy. *Biochim. Biophys. Acta*, **1462**, 157–183.
41. Fragneto, G., Bellet-Amalric, E. & Graner, F. (2002). Neutron and X-ray studies of lipid bilayers. In *Research Signpost* (Heitz, F., ed) Membrane Interacting Peptides and Proteins.
42. Fragneto, G., Charitat, T., Graner, F., Mecke, K., Perino-Gallice, L. & Bellet-Amalric, E. (2001). A fluid floating bilayer. *Europhys. Lett.* **53**, 100–106.
43. Bechinger, B., Kinder, R., Helmle, M., Vogt, T. C., Harzer, U. & Schinzel, S. (1999). Peptide structural analysis by solid-state NMR spectroscopy. *Biopolymers*, **51**, 174–190.
44. Aisenbrey, C., Prongidi-Fix, L., Chenal, A., Gillet, D. & Bechinger, B. (2009). Side chain resonances in static oriented proton-decoupled ^{15}N solid-state NMR spectra of membrane proteins. *J. Am. Chem. Soc.* **131**, 6340–6341.
45. Lambotte, S., Jasperse, P. & Bechinger, B. (1998). Orientational distribution of α-helices in the colicin B and E1 channel domains: a one and two dimensional ^{15}N solid-state NMR investigation in uniaxially aligned phospholipid bilayers. *Biochemistry*, **37**, 16–22.
46. Progidi-Fix, L. (2005). *Structural and thermodynamic investigations of membrane associated polypeptides and peptide/DNA transfection complexes*. PhD Thesis. http://eprints-scd-ulp.u-strasbg.fr:8080/465/01/PhD_ProngidiFix.pdf, 110 pp.
47. Wang, J., Rosconi, M. P. & London, E. (2006). Topography of the hydrophilic helices of membrane-inserted diphtheria toxin T domain: TH1–TH3 as a hydrophilic tether. *Biochemistry*, **45**, 8124–8134.
48. Lai, B., Zhao, G. & London, E. (2008). Behavior of the deeply inserted helices in diphtheria toxin T domain: helices 5, 8, and 9 interact strongly and promote pore formation, while helices 6/7 limit pore formation. *Biochemistry*, **47**, 4565–4574.
49. Chenal, A., Vernier, G., Savarin, P., Bushmarina, N. A., Geze, A., Guillain, F. *et al.* (2005). Conformational states and thermodynamics of α-lactalbumin bound to membranes: a case study of the effects of pH, calcium, lipid membrane curvature and charge. *J. Mol. Biol.* **349**, 890–905.
50. Finkelstein, A., Oh, K. J., Senzel, L., Gordon, M., Blaustein, R. O. & Collier, R. J. (2000). The diphtheria toxin channel-forming T-domain translocates its own NH_2-terminal region and the catalytic domain across planar phospholipid bilayers. *Int. J. Med. Microbiol.* **290**, 435–440.
51. Oh, K. J., Senzel, L., Collier, R. J. & Finkelstein, A. (1999). Translocation of the catalytic domain of diphtheria toxin across planar phospholipid bilayers by its own T domain. *Proc. Natl Acad. Sci. USA*, **96**, 8467–8470.
52. Sandvig, K., Tonnessen, T. I., Sand, O. & Olsnes, S. (1986). Requirement of a transmembrane pH gradient for the entry of diphtheria toxin into cells at low pH. *J. Biol. Chem.* **261**, 11639–11644.
53. Hudson, T. H., Scharff, J., Kimak, M. A. & Neville,

D. M., Jr (1988). Energy requirements for diphtheria toxin translocation are coupled to the maintenance of a plasma membrane potential and a proton gradient. *J. Biol. Chem.* **263**, 4773–4781.
54. Trujillo, C., Ratts, R., Tamayo, A., Harrison, R. & Murphy, J. R. (2006). Trojan horse or proton force: finding the right partner(s) for toxin translocation. *Neurotox. Res.* **9**, 63–71.
55. Tamayo, A. G., Bharti, A., Trujillo, C., Harrison, R. & Murphy, J. R. (2008). COPI coatomer complex proteins facilitate the translocation of anthrax lethal factor across vesicular membranes *in vitro*. *Proc. Natl Acad. Sci. USA*, **105**, 5254–5259.
56. Bechinger, B. & Lohner, K. (2006). Detergent-like actions of linear amphipathic cationic antimicrobial peptides. *Biochim. Biophys. Acta*, **1758**, 1529–1539.
57. Henriques, S. T., Melo, M. N. & Castanho, M. A. (2006). Cell-penetrating peptides and antimicrobial peptides: how different are they? *Biochem. J.* **399**, 1–7.
58. Bechinger, B. (2008). A dynamic view of peptides and proteins in membranes. *Cell. Mol. Life Sci.* **65**, 3028–3039.
59. Lemichez, E., Bomsel, M., Devilliers, G., vanderSpek, J., Murphy, J. R., Lukianov, E. V. *et al*. (1997). Membrane translocation of diphtheria toxin fragment A exploits early to late endosome trafficking machinery. *Mol. Microbiol.* **23**, 445–457.
60. Lemichez, E. & Boquet, P. (2003). To be helped or not helped, that is the question. *J. Cell Biol.* **160**, 991–992.